RSC Advances

ROYAL SOCIETY OF CHEMISTRY

www.rsc.org/advances

RSC Advances

Cite this: DOI: 10.1039/c0xx00000x

ARTICLE TYPE

www.rsc.org/xxxxxx

Photochemically assisted one–pot synthesis of PMMA embedded silver nanoparticles: Antibacterial efficacy and water treatment

Shubhangi Borse,[†] MayurTemgire,[‡] Ayesha Khan[†] and Satyawati Joshi *[†]

Received (in XXX, XXX) XthXXXXXXXXX 20XX, Accepted Xth XXXXXXXXX 20XX
DOI: 10.1039/b000000x

One–pot synthesis of polymer embedded silver nanoparticles (AgNPs) by UV irradiation method was performed and thoroughly characterized. Electron microscope analysis revealed that AgNPs (17.30 nm) were embedded into PMMA matrix. High–resolution transmission electron microscopy (HRTEM) study indicates that of silver–poly (methyl methacrylate) (Ag–PMMA) nanocomposite exhibited internal high ordered lattice fringes of Ag (111) lattice plane. Ag–PMMA nanocomposite had a lower tendency to agglomerate than borohydride reduced AgNPs evaluated by stability experiment. The nanocomposite shows zeta potential –63.9 mV confirming high stability of nanocomposite. Organic reagent test reveals that the synthesized nanocomposite contains more amounts of Ag^0 state particles and less amount Ag^+ ion. Fourier transform infrared spectroscopy (FTIR) studies evidenced that carbonyl group of PMMA binds with AgNPs. The nanocomposite exhibited excellent antibacterial performance against Gram–negative *Escherichia coli*, *Pseudomonas aeruginosa* and Gram–positive, *Staphylococcus aureus*. Moreover, the possible mechanism for the antibacterial activity of Ag–PMMA nanocomposite with *E. coli* bacteria has been discussed. In addition, Ag–PMMA nanocomposite solution was loaded on membrane (treated membrane) for water treatment application and characterized by spectroscopy techniques. Sludge water was passed through treated membrane and the effluent water analyzed for viable bacteria. Deactivation of bacteria by percolation through treated membrane occurred. Consequently, the filter effluent contains dead bacteria, which indicates that treated membrane exhibits antibacterial properties. Interestingly, Microwave plasma –atomic emission spectrometry (MP–AES) analysis estimated that the silver loss from treated membrane was less than 0.1 ppm.

Introduction

Water is the number one global risk of highest impact in the next ten years, according to the 2015 Global Risk Report. Analytical studies have projected our global demand for water will exceed available supply by 40% in 2030, and by 2050, an estimated $63 trillion of global Gross Domestic Product (GDP) will be put at risk under 'business as usual' water management practices and productivity.[1] Natural waters are frequently contaminated mostly through discharges of sewage and industrial wastewater, which encompass toxic or carcinogenic impurities causing numerous public health complications. Generally chlorination, ozonation and UV–treatment methods are being used for water disinfection.[2–6]

The basic aim of water treatment is to remove undesired constituents from water.[6] The use of membrane technology in water treatment has gained impetus for treating microorganism, particulates and organic materials that contaminate water. Membrane based technology is a promising disinfection method in which microorganisms are retained without any harmful chemical treatment. Membrane technology is well established for water treatment because it is reliable and largely automated process. Membranes deliver a physical barrier for such constituents based on their size, permitting use of unconventional water sources.[7] However, biofouling is a serious problem that occurs during membrane filtration process due to deposition of microbial cells or other organic matter present in the feed stream.[8] Nanotechnology embraces great potential in advancing water and waste water treatment to improve treatment effectiveness and to increase water supply through safe use of unconventional water sources.[6,7] Incorporation of nanomaterials into membranes offers a great prospect to improve the membrane permeability, fouling resistance, mechanical and thermal stability, in addition to render new functions for contaminant degradation and self–cleaning.[9,10] Particularly, biocidal silver nanoparticles (AgNPs) are effective disinfectants and work for a wide spectrum of bacteria and viruses.[11-13]AgNPs have been used previously in water filtration applications, as they prevent bacterial fouling of membrane filters. Compared to AgNPs, immobilized AgNPs are physico–chemically more stable as they are less prone to aggregation and oxidation when exposed to the aqueous media.[14] Attributable to this, polymer engineered AgNPs impregnated membrane are currently being explored due to effective removal of bacteria. Mohammad and his co–workers have synthesized nanohybrid polusulfone membrane with silver–decorated graphene nanoplates and this synthesized nanohybrid membranes show excellent antibacterial properties.[15] Mauter and Zodrow groups demonstrated that the synthesized nano–Ag has been surface grafted on polymeric membranes to inhibit bacterial attachment and biofilm formation on the membrane surface as well as inactivate viruses.[16,17] Cao et al., investigated antibacterial effect of AgNPs in polyethersulfone membrane against *S. aureus*, *S. albus* and *E. coli*.[18] Diagne et al., modified commercially available polyethersulfone membrane by polyelectrolyte multilayer modification method using poly (styrenesulfone), poly (diallyldimethylammonium chloride) and AgNPs, which show resistance to biofouling and inhibit bacterial growth.[19] Smith et al. have shown that AgNPs embedded in the ceramic porous media improve the removal and disinfection of *E. coli*.[20] Morones et al., studied the activity of nanoscale silver particles embedded

in a carbon matrix towards four types of Gram–negative bacteria and they found that all types of Gram–negative bacteria are inactivated due to interaction with the AgNPs.[21]Taurozzi et al. found that when polysulfone (PSf) membranes are formed with AgNPs included in the casting solution by *ex situ* and *in situ* reduction methods, it increased water permeability.[22] Polymer engineered AgNPs has attracted interest due to its antibacterial properties. Jang reported the synthesis of Poly [2–(tert–butylaminoethyl) methacrylate] (PTBAM) embedded AgNPs by radical–mediated dispersion polymerization. The fabricated Ag/PTBAM nanofibers show enhanced antibacterial activities against both Gram–negative *E. coli* and Gram–positive *S. aureus*.[23] An et al. studied the capability of electrospun chitosan–polyethylene oxide membrane impregnated by silver for removal of *E. coli*.[24] Poly (methyl methacrylate) (PMMA) has been extensively used in medical and dental application due to its biocompatible nature. Alt et al. described the *in vitro* antibacterial activity of nanosilver against multi resistant bacteria and the *in vitro* cytotoxicity of AgNPs loaded into PMMA bone cement.[25]

Here, our study focuses on the *in–situ* synthesis of AgNPs in polymer matrix through photo–assisted processes. Taking advantage of beneficial properties of UV rays and antibacterial effects of Ag, we have synthesized Ag–PMMA nanocomposite for water treatment. In the present study, PMMA was used as polymer substrate to encapsulate AgNPs. Photochemical fabrication is one of the most powerful simple, cost–effective, and convenient technique for the synthesis of metal nanoparticles. In principle, the photochemical approach is the generation of M^0 in such conditions that their precipitation is thwarted. M^0 can be formed through direct photoreduction of a silver source, silver salt or complex, or reduction of silver ions using photochemically generated intermediates, such as radicals. In this one–step approach, we report a strategy involving the photoinduced formation of homogeneous AgNPs in a polymer (PMMA) stemming from a cross–linking photo–polymerization of a methyl methacrylate monomer. The effect of MMA concentration in Ag–PMMA formation has been investigated. In addition, antibacterial properties of Ag–PMMA nanocomposite have been evaluated against *E. coli*, *P. aeruginosa* (Gram–negative) and *S. aureus* (Gram–positive) bacteria using antibacterial activity, growth kinetics and minimum inhibitory concentration (MIC). The synthesized Ag–PMMA nanocomposite exhibited excellent antimicrobial activity toward Gram–negative and Gram–positive bacteria. We have made an attempt to explore the possibility of fabricated Ag–PMMA nanocomposite as antibacterial agent for water treatment. Sludge water was collected from Mula river (Pune, India) which contains Gram–positive as well as Gram–negative bacteria. To test the bactericidal action, colloidal solution of the nanocomposite was loaded on membrane (treated membrane). Then sludge water was passed through treated membrane and effluent water was analyzed for viable bacteria. Deactivation of bacteria in sludge water occurred by percolation followed by death confirmed by antibacterial activity and microbial slide test. The membrane was characterized in terms of surface morphology by field emission scanning electron microscope (FE–SEM) studies.

Experimental

Materials

All the chemicals used were of analytical grade. Silver nitrate ($AgNO_3$) (Fluka, Switzerland), methyl methacrylate (MMA) (Merck, India) and dioctyl sodium sulfosuccinate (AOT), 2, 2–Azobis (isobutyronitrile) (AIBN) and propan–2–ol were obtained from Merck, India. All the reagents were of analytical grade and used as received, without further purification. Milli–Q deionized water was used for synthesis. To test bacterial growth, *E. coli* (ATCC 11775), *P. aeruginosa* (ATCC 47085) and *S. aureus* (ATCC 12600) were purchased. Millipore PVDF membrane of 13 mm diameter with 0.22 μm pore size were purchased from Merck (India) and for sludge water sample membrane testing filtration unit was used.

Synthesis of Ag–PMMA nanocomposite

In a typical procedure, total volume of 100 mL was made by adding silver precursor of 88.6 mL ($AgNO_3$, 10^{-3} M), 2% AOT (10 mL), AIBN (0.047 g), isopropanol 1.2 mL (0.2 M), MMA of (0.02 M) 0.2 mL, were added in Milli–Q water. Low pressure Hg lamps of 200 W (Srinivasan–Griffin Rayonet, JSGW type) were used as a UV light source and the solution was irradiated for 24 h. This instrument comprised of eight ultraviolet tubes of wavelength 253.7 Å fitted in a heavy metal enclosure with an in built magnetic stirrer. The incident photon number of 253.7 nm light (determined by a tris (oxalato) ferrate (111) actinometer) was 5.0×10^{15} cm^2 s^{-1}. When the reaction solution was irradiated with UV light, the room temperature was controlled by using water circulation. After UV irradiation, the solution color changed from colorless to yellow, indicating the formation of PMMA embedded nanoparticles.

Organic reagent test

0.1 M stock solution of Rhodanine was prepared in water. 10μL of Rhodanine (0.1M) solution was added to 5 mL $AgNO_3$ (0.1M) solution. After regular time interval (5 minute, 7 h and 24 h) UV–Visible spectral study of these solutions was performed. Same experimental procedure was performed for synthesized Ag–PMMA nanocomposite.

Effect of MMA monomer volume on synthesis of nanocomposite

Total volume of 100 mL was made by adding silver precursor of 88.6 mL ($AgNO_3$, 10^{-3} M), 2% AOT (10 mL), AIBN (0.047 g), isopropanol 1.2 mL (0.2 M) , MMA of (0.02 M) 0.2/0.4/0.6/0.8/1 mL, were added in Milli–Q water. Low–pressure Hg lamps of 200 W were used as a UV light source and the solution was irradiated for 24 h. After UV irradiation, the solution color changed from colorless to yellow, indicating the formation of PMMA embedded nanoparticles.

Borohydride reduced silver nanoparticles

Silver nanoparticles (AgNPs) were prepared by reduction of 10 mL of 1 mM silver nitrate ($AgNO_3$) with 30 mL of 2 mM ice–cold sodium borohydride solution ($NaBH_4$). Briefly, the solution of silver nitrate was vigorously stirred with the sodium borohydride solution for an hour at room temperature. Finally, the solution color changed from colorless to yellow, indicating the formation of AgNPs.

Ag–PMMA nanocomposite loaded membrane

The membrane was moistened by dipping it in a 50% ethanol–water mixture. The membrane was then placed into the membrane holder. The membrane holder was then attached to the syringe and 10 mL of Ag–PMMA nanocomposite solution was passed through the membrane (treated membrane). The membrane traps the Ag–PMMA nanocomposite on upper side of membrane. The Ag–PMMA nanocomposite loaded membrane was then removed from the holder and dried.

Analysis for silver in effluent

The effluent after passing through the treated membrane was analyzed for silver content by MP–AES. 9 mL of nitric acid (10%) was added to 1mL effluent. This solution was kept overnight. The samples were then analyzed for total silver content by MP–AES. The sample measurements were done in triplicates. The values reported were based on a calibration curve using an Ag MP–AES standard. The emission Ag line is at 328.06 nm. The silver loss from the treated membrane in 10 mL of effluent was determined from the MP–AES values for silver concentration in the effluent water. This value was expressed as a percentage of the total silver mass contained in the treated membrane, as determined by MP–AES measurements.

To quantify the amount of silver content in treated membrane analysis was performed by an acid digestion of the membrane and analyzed the amount of dissolved silver using MP–AES. Briefly, approximately 100 mg of dried membrane was reacted with 5 mL of 70% nitric acid in 5 mL of water and then boiled until it disintegrated. After cooling, the suspension was filtered through a glass filter. The silver content of the effluent was measured with MP–AES.

Instrumentation

The optical absorption spectra of colloidal solutions were recorded on UV–VIS 1800 (Shimadzu) spectrophotometer. FTIR spectra were recorded on Bruker Tensor 27 instrument. High resolution transmission electron microscopic (HRTEM) images were taken using JEOL – JEM 2100 HRTEM operated on 200 kV, for which the samples were prepared by dropping 2µLnanocompositesolution onto a 400–mesh icon carbon–coated copper grid and wicking off the excess sample with filter paper after 30 seconds and drying at room temperature. Crystallinity and crystal phases of the synthesized nanocomposite were determined by a Philips PW 1840 powder X–ray diffractometer (XRD) with CuKα radiation (l = 1.54178 Å) with Bragg angle ranging from 20 to 80°. The particle size was calculated from full width at half maximum (FWHM) of the diffracted lines using Scherrer formula. The thermal decomposition pattern of the sample was studied by thermo gravimetric analysis (TGA) using a TGA 2050 analyzer. The TGA was done from room temperature to 900 °C in nitrogen atmosphere. The heating rate was maintained at 10°C min^{-1}. Dynamic light scattering (DLS) hydrodynamic size and zeta potential of the Ag–PMMA nanocomposite was obtained on Malvern ZetasizerNano ZS instrument. Briefly, the samples were loaded into a pre–rinsed folded capillary cell and a voltage of 150 and 100 V was applied. The zeta potential measurements were made in triplicates. The presence of Ag–PMMA nanocomposite on membrane was established by measuring the reflectance spectra of the treated membrane on UV–visible diffuse reflectance spectrophotometer (DRS, JASCO V–670). Microwave plasma–atomic emission spectrometry (MP–AES, Agilent 4100) was used for the quantification of silver content. Optical microscopic images were taken on Leica DM 2500 microscope. Microstructures of samples were observed by FE–SEM, (Nova NanoSEM 450). The samples were drop casted on silicon wafer and coated with chromium/gold sputtering for conductivity.

Antibacterial test

Ag–PMMA nanocomposite was tested against *E. coli*, *P. aeruginosa* and *S. aureus* by well diffusion method. Bacterial suspension was cultured in nutrient broth medium at 37^0 C for 24 h. Drops of bacterial suspension (100 µL) were added onto the surface of the agar and spread using sterile glass spreader. 7 mm diameter of well was made on nutrient agar plate with the help of gel puncture. 25 µL of Ag–PMMA nanocomposite and PMMA solution (without Ag) were added to the well, and then the plates were incubated in incubator for 37 ^{0}C for 24 h. Same procedure was followed to test antibacterial activity of treated membrane. The standard error was calculated using three replicates of experiments.

The minimum inhibitory concentration (MIC) test was performed as follows. Sterilized LB agar solutions (5 mL) were inoculated with bacterium (10^5–10^6 CFU). Then synthesized nanocomposite was added to the bacteria suspensions at different concentrations (5, 10, 15, 20 and 25 µL) and incubated at 37 ºC with shaking at 150 rpm for 24 h. Bacterial growth was measured as an increase in absorbance at 600 nm. The experiments also included a positive control (a flask containing the nanocomposite and nutrient media) and a negative control (flask containing inoculums and nutrient media). Three replicates of this experiment have been performed.

For the kinetic test, *E. coli*, *P. aeruginosa* and *S. aureus* suspensions were prepared. The culture medium of each bacterium was inoculated with bacteria and incubated overnight at 37 °C. Bacterial growth rates were measured by monitoring the optical density at 600 nm (OD_{600}) using a spectrophotometer. The incubated bacteria were inoculated in to the fresh media and grown at 37 °C with 200 rpm of shaking to an OD_{600} of 0.1. Various concentrations of Ag–PMMA nanocomposite (from 1 to 25 µL) were then added to the culture, and the OD_{600} was measured over time. This experiment has been repeated three times.

Ag–PMMA nanocomposite interaction with *E. coli* bacteria

To demonstrate the mechanism of the biocidal action of Ag–PMMA nanocomposite, *E. coli* bacterial cells (each at 10^6–10^7 CFU ml^{-1}) were treated with Ag–PMMA nanocomposite (25 µL) for 6 h. Untreated *E. coli* cells were used as control. The treated cells were harvested by centrifugation (10000 rpm, 10 min.) and washed thrice with Milli–Q water to remove the loosely bound Ag–PMMA nanocomposite over the bacterial surface. A series of pre–treatment steps were followed for FE–SEM analysis. Primary fixation of bacterial cells was achieved using 2.5% glutaraldehyde for 1 h. Then samples were subsequently dehydrated with a graded ethanol series (30%, 50%, 70%, 90%, 95% and 100%).

Results and Discussion

The synthesis of PMMA embedded AgNPs was accomplished by UV irradiation of the solution of silver nitrate, AOT and MMA. As a result of UV–irradiation, simultaneous polymerization and reduction of metallic silver took place. Under UV irradiation, polymerization of MMA to PMMA using AIBN (reductant radical inhibitor) occurred. Also, AIBN partly undergoes electron transfer with silver salt, thus reduction of metallic silver occurred in the presence of UV irradiation. The reduced silver atoms were stabilized by AOT surfactant by coordinating sulfonic group of AOT.[26] The stabilized AgNPs have strong interaction with oxygen in C=O groups of PMMA polymer. High interaction of AgNPs with carbonyl oxygen (C=O) than that of the C–O in ester functional group is due to the higher negativity of the charge density for the C=O than C–O in the polymer matrix.[27, 28]

To clarify the morphology of polymer embedded AgNPs, TEM analysis was carried out. Figure 1 depicts TEM image of the synthesized nanocomposite. TEM analysis confirmed that

AgNPs of average 17.30±0.4 nm in diameter were finely embedded throughout the polymer nanorods. Ag–PMMA nanocomposite shows average diameter of 0.4 µm and 2.2 µm lengths with standard deviation of ±2.4 nm (Figure S1, Supporting Information). Additionally, the synthesized nanocomposite possesses a smooth surface morphology (Figure 1a to 1g), which indicates that the AgNPs were not located on the surface but instead were embedded inside the PMMA nanorods. To gain further insight into the morphology, HRTEM was performed of polymer embedded AgNPs (Figure 1h). The synthesized nanocomposite exhibited internal high ordered lattice fringes with the lattice spacing of 0.23 nm, corresponding to the (111) lattice plane of Ag. The interplanar distance of the nanosilver (111) plane is in good agreement with the (111) d–spacing of bulk Ag (0.2359 nm).[29] The favored alignment of AgNPs in PMMA is at (111) plane. This can be elucidated from a perspective of thermodynamics since the preferred orientations of solid particles are known to be perpendicular directions to the planes of lowest surface energy, which corresponds to the most densely packed planes for metallic materials.[30,31] The SAED pattern confirms the polycrystalline nature of the AgNPs (Figure 1i).

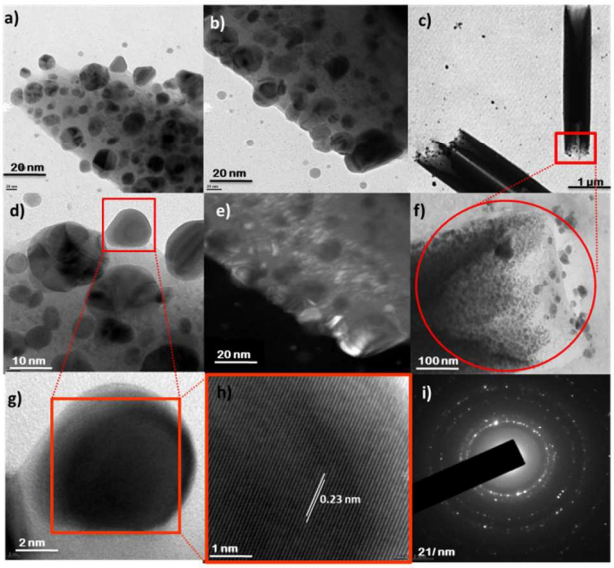

Figure 1 TEM micrographs of (a, g) PMMA embedded AgNPs with bright field (a, b, c, d, f and g) and dark field (e). (h) HR–TEM image and (i) SAED pattern of polymer embedded AgNPs.

The crystalline character of Ag–PMMA nanocomposite was supported from XRD analysis (Figure S2, Supporting Information). The synthesized nanocomposite exhibits the four distinct diffraction peaks at 2Θ values at 38.1^0, 44.3^0, 64.4^0, and 77.3^0 correspond to the (111), (200), (220), and (311) planes of Ag crystal, respectively (JCPDS card number 4–0783). All the diffraction peaks can be indexed to the planes of face–center–cubic (fcc) silver, with a lattice constant of about 4.08 Å.[32] The XRD results demonstrated that the preferred growth plane of the particles is the (1 1 1) lattice plane. The crystallite size (34.4 nm, average particle size) the synthesized nanocomposite was calculated from FWHM of the peaks of silver by Scherrer equation.

The size distribution of Ag–PMMA nanocomposite was measured by DLS. The average particle size obtained from DLS data is 178 nm (Figure S3, Supporting Information). DLS analysis indicates that the effective hydrodynamic diameter of Ag–PMMA nanocomposite measured by DLS is larger than the hard core sizes measured by TEM. DLS analysis includes the ligand shell and determines the hydrodynamic size. While TEM analysis provides the information of the metallic core of particle.[33] Dynamic Light scattering (DLS) is a technique for measuring the size of particles typically in the sub micron region. DLS measures Brownian motion and relates this to the size of the particles. Brownian motion is the random movement of particles due to the bombardment by the solvent molecules that surround them. Normally DLS is concerned with measurement of particles suspended within a liquid. The larger the particle, the slower the Brownian motion will be. Smaller particles are moved further by the solvent molecules and move more rapidly. The velocity of the Brownian motion is defined by a property known as the translational diffusion coefficient (D). The size of a particle is calculated from the translational diffusion coefficient by using the Stokes–Einstein equation 1;

$$d(H) = \frac{kT}{3\pi\eta D} \qquad (1)$$

Where,
$d(H)$ = hydrodynamic diameter
D = translational diffusion coefficient
k = Boltzmann's constant
T = absolute temperature
η = viscosity

The diameter measured in DLS signifies how a particle diffuses within a fluid so it is referred to as a hydrodynamic diameter. It is the diameter of a sphere that has the same translational diffusion coefficient as the particle. The translational diffusion coefficient mainly depends on the size of the particle core, surface structure, concentration, type of ions in the medium and ionic strength of the medium as well. Any change to the surface of a particle that affects the diffusion speed will correspondingly change the apparent size of the particle. An adsorbed polymer layer projecting out into the medium may reduce the diffusion speed. The nature of the surface and the polymer, as well as the ionic concentration of the medium can affect the polymer conformation, which in turn can change the apparent size by several nanometres.[33]

DLS measures the hydrodynamic diameter of the whole solution components viz. *in situ* AgNPs, including the Ag core, capping agents and any other molecules sorbed to the surface, and layers of solvent molecules that are associated with the NPs during Brownian motion. These components are assumed to conform to a spherical geometry. During DLS measurements, Raleigh scattering dictates that the light intensity scattered by a NP is proportional to its diameter raised to the sixth power, and thus larger diameter particles will dominate the intensity signal.[33]

Using DLS we get the hydrodynamic radius of the particle whereas by TEM we get an estimation of the projected area diameter. According to DLS theory, when a dispersed particle moves through a liquid medium, a thin electric dipole layer of the solvent adheres to its surface. This layer influences the movement of the particle in the medium. Thus, the hydrodynamic diameter gives us information of the inorganic core along with any coating material and the solvent layer attached to the particle as it moves under the influence of Brownian motion. While estimating size by TEM, due to difference in sample preparation method, hydration layer is absent hence, we get information only about the inorganic core. The projected area diameter estimated by TEM is theoretically defined as the area of a sphere having the same area as the projected area of the particle resting in a stable

position. Sometimes due to poor contrast in TEM, the size measurement of the coating layer if present could be underestimated or missed. Hence, the hydrodynamic diameter is always greater than the size estimated by TEM.

The Ag–PMMA nanocomposite was further examined by TGA in order to obtain quantitative information on the silver content (Figure S4, Supporting Information). It was observed from TGA curve that two dominant weight losses of the sample occurred in temperature region between 158–506 °C (Figure S4, Supporting Information). There were almost no weight losses after 506°C. The total weight loss was 90.77 %, resulting in a silver content of 9.33 %. Marning and coworker also reported that the unsaturated ends (PMMA) are responsible for two step weight losses around 180 °C and 270 °C for silver–polymer nanoparticles. They observed two step weight losses mainly in the temperature range from 158 to 506 °C with silver–polymer nanoparticles.[29] Earlier study has reported that the thermal stability of PMMA is improved due to presence of silver. The presence of small amount of Ag in polymer matrix confines the motion of polymer chains, which renders improved thermal stability.[35]

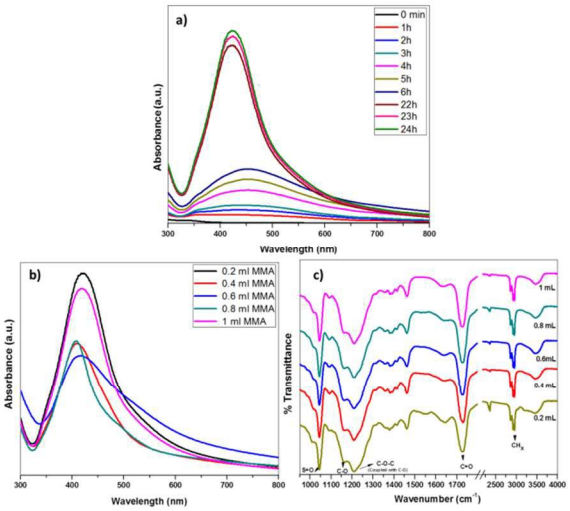

Figure 2 (a) UV–Visible spectra of Ag–PMMA nanocomposite as a function of UV irradiation with time. (b) UV–Visible and (c) FTIR spectra of Ag–PMMA nanocomposite with increasing volume of MMA monomer.

The characteristic surface plasmon resonance (SPR) spectra of metal nanoparticles provide a convenient tool to monitor their formation and gain insight into the particle size and shape. The optical property of the Ag–PMMA nanocomposite was analyzed by UV–Visible spectroscopy. Figure 2a depicts the absorption band at 421 nm, which is a characteristic SPR band for AgNPs. It is known that SPR absorption of nanoparticles is sensitive to geometric parameters, aggregation and surrounding matrix. The SPR band starts to appear after 1 h of irradiation and grows with time. Formation of Ag–PMMA nanocomposite was completed within 24 h (Figure 2a). While further irradiation upto 48 h show no change in SPR band. This result indicates that 24 h is the optimum irradiation time for synthesis of Ag–PMMA nanocomposite.

In order to verify the role of AOT in the synthesis, a blank system containing only silver ion and MMA (without AOT) was examined. There was no formation of Ag–PMMA nanocomposite and no color change of solution. From this experiment, it can be concluded that AOT acts as a stabilizing agent to prohibit aggregation of silver. Also to ensure the compatibility of solutions, it was checked that AOT and MMA with AIBN do not interacting before irradiation. More information about the role of AOT surfactant is provided in Supporting Information section (Figure S5, Supporting Information).

The effect of MMA monomer volume on the formation Ag–PMMA nanocomposite was studied by UV–Visible and FTIR spectroscopy (Figure 2). UV–Visible study demonstrates that as the volume of MMA monomer increases (0.2 to1 mL), SPR band of Ag–PMMA nanocomposite becomes broader (Figure 2b). This result indicates that 0.2 mL volume of MMA is the optimum volume for the synthesis of Ag–PMMA nanocomposite. FTIR spectra of Ag–PMMA nanocomposite presented in Figure 2c, shows a broad band around 3399 cm^{-1}, indicating the presence of −OH group. Prominent bands at 2955, 2928 and 2867 cm^{-1} attributed to C–H_X bending and stretching vibration.[36-39] The strong bands at 1728 cm^{-1} and 1650 cm^{-1} ascribed to carbonyl stretching vibration and C=C stretching vibration, respectively.[36,37] The bands at 1460 cm^{-1} and 1385 cm^{-1} associated with CH_3 and C–H bending modes. The band at 1211 cm^{-1} corresponds to C–C–O coupled with C–O stretch.[36,37] Whereas bands at 1160 cm^{-1} and 749 cm^{-1} accredited from C–O symmetrical stretching modes of ester groups from PMMA and rocking vibration of CH_2, respectively.[38] The sharp band at 1044 cm^{-1} assigned to the S=O stretching vibration of the sulfonate group present in the AOT molecules.[26] However, the strong bands at 1728 cm^{-1}corresponds to carbonyl stretching vibration, which became sharper with increase in volume of MMA monomer. FTIR study demonstrated that binding takes place through carbonyl groups from PMMA with AgNPs.

To check the stability, an aggregation test for borohydride reduced silver nanoparticles (AgNPs–B) and Ag–PMMA nanocomposite in presence of light and absence of light (dark) was carried out for 5 days (Figure 3). Under white–light (60 W) conditions, it was observed that the color of AgNPs–B turned from yellow to green after 5 days. The corresponding UV–Visible spectra of AgNPs–B show SPR bands at 401 nm (intensity decreased) and 650 nm, suggesting that AgNPs were aggregated (Figure 3a).[40, 41] This result indicates that aggregation process was light sensitive. While the AgNPs–B stored in dark exhibited no color change as indicated with no shift in SPR band position. Under the same conditions, aggregation test for Ag–PMMA nanocomposite was carried out. UV–Visible spectra of Ag–PMMA nanocomposite were nearly unchanged when stored either in the dark or in the light for 5 days (Figure 3b). Based on these data, it can be concluded that Ag–PMMA nanocomposite has a lower tendency toward aggregation than AgNPs–B because polymer substrate prevented aggregation of the embedded AgNPs.[42]The stability was also checked using zeta potential. Negative/positive zeta potential value indicates the degree of repulsion between charged particles in a nanosuspension. More negative zeta potential value indicates stronger electrostatic repulsion force between nanoparticles and better stability. Ag–PMMA nanocomposite shows zeta potential –63.9 mV confirming high stability of nanocomposite (Figure S6, Supporting Information).

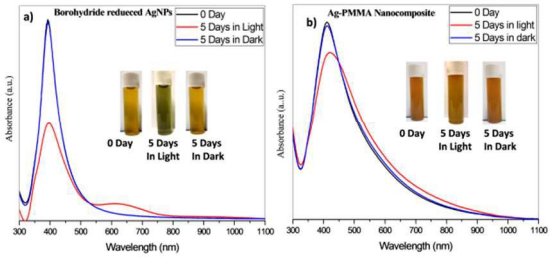

Figure 3 UV–Visible spectra of (a) AgNPs–B, and (b) Ag–PMMA nanocomposite. The spectra obtained when the sample was freshly synthesized (black line), stored in dark condition (blue line) and stored with white light irradiation (red line). The inset pictures represent the sample solution under different conditions.

An organic reagent test was performed to examine the oxidation of Ag–PMMA nanocomposite. It is reported that metallic silver can be oxidized to silver ion.[43]Particularly, for the detection of silver salts, rhodanine is used because it is a selective and sensitive reagent towards silver ion. After addition of aqueous solution of rhodanine into silver nitrate ($AgNO_3$) solution, immediate color change occurred (colorless to light yellow) which gradually further changed into brown–black precipitate due to the formation of Ag–Rhodanine complex (Figure 4). Stephen and co–workers reported that precipitation occurred due to involvement of acidic imino–hydrogen group of rhodanine by silver ion.[44] Whereas same rhodanine solution when added into Ag–PMMA nanocomposite solution shows no color change, only color became faint after 24 h without any precipitation. This result indicates that less amount of AgNPs in polymer matrix was oxidized (Ag^+) since most of particles exist in Ag^0 state.

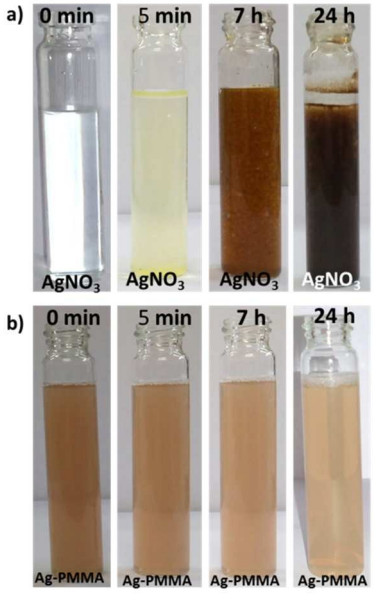

Figure 4 Photographic images of (a) silver nitrate and (b) Ag–PMMA nanocomposite solution as a function of rhodanine addition with time.

Antibacterial activity of Ag–PMMA nanocomposite

The antibacterial activity of Ag–PMMA nanocomposite was investigated against *E. coli*, *P. aeruginosa* and *S. aureus* using an agar–gel method. The antibacterial properties were measured by evaluating the zone of inhibition (ZoI) around the disk after incubation at 37 °C (Figure S7, Supporting Information). The diameter of the zone of inhibition for the Ag–PMMA nanocomposite (25 µL) was 14± 0.25, 13± 0.48 and 10± 0.36 mm against *E. coli, P. aeruginosa* and *S. aureus* respectively (Figure S7b, Supporting Information). However, PMMA system (without Ag) shows no zone of inhibition against *E. coli, P. aeruginosa* and *S. aureus.* (Figure S7a, Supporting Information). These results indicated that the Ag–PMMA nanocomposite exhibited an antibacterial property. Jang and coworker have found similar results, that the nanometer–sized PTBAM polymer nanofibers provided a large surface area for more effective antimicrobial performance.[23]

To study the growth kinetics of *E. coli*, *P. aeruginosa* and *S. aureus* bacteria with Ag–PMMA nanocomposite a bacterial inhibition growth curve was used. The dynamics of bacterial growth curve was monitored in liquid LB broth. Time–dependent changes in the bacterial growth were monitored at a regular interval of 2 h (upto 12 h) by measuring the OD (at 600 nm) of the control (without Ag–PMMA nanocomposite) and bacterial solutions supplemented with Ag–PMMA nanocomposite (0.5 µg/mL) was shown in Figure S8, Supporting Information. Bacterial cell growth enhances the turbidity of the liquid medium and as a result, the absorption increases. Ag–PMMA nanocomposite caused a growth delay of the bacterial cells and the slope of the bacterial growth curve continuously decreased with time (Figure S8, Supporting Information). An MIC test was also performed to quantitate antibacterial activity of the Ag–PMMA nanocomposite against *E. coli*, *P. aeruginosa* and *S. aureus* bacteria (Figure S9, Supporting Information). The MIC value for Ag–PMMA nanocomposite was found to be in the range of 0.032 to 0.125 µg/ ml for *E. coli*, *P. aeruginosa* and *S. aureus* bacteria. These results demonstrate that the Ag–PMMA nanocomposite inhibit the bacterial growth.[45]

Antibacterial activity (MIC and growth curve, ZoI) results show that Ag–PMMA nanocomposite was more lethal to *E. coli* and *P. aeruginosa* than to *S. aureus* bacteria. This happens due to the fact that, Gram positive bacteria have a large number of free amines and carboxyl groups on their surfaces, while Gram negative have the capability to protect themselves from the antimicrobial agents. Also due to the different strength of antibacterial activities of Ag–PMMA nanocomposite towards Gram positive (*E. coli* and *P. aeruginosa)* and Gram negative (*S. aureus)* bacteria arises due to the difference in cell structure of bacteria. Gram positive bacteria possess cell wall although Gram negative bacteria do not have cell wall. Also both bacteria have different physiology, activity and metabolic rate.[46]

Ag–PMMA nanocomposite interaction with *E. coli* bacteria

The precise mechanism of action of silver on the microbes is still not recognized. Literature reports that, AgNPs first get attached to the cell membrane and penetrate inside the bacteria.[47]In general silver has a greater propensity to react with sulfur– or phosphorus–containing soft bases (R–S–R, R–SH, RS–, or PR_3). Thus, sulfur–containing proteins in the cell membrane and inside the cells phosphorus–containing elements like DNA are potential binding sites for AgNPs. The AgNPs preferably attack respiration chain, cell division finally leading to cell death.[48]

In order to investigate the interaction behavior of Ag–PMMA nanocomposite with *E. coli* bacteria, FE–SEM imaging was done (Figure 5). *E. coli* bacterial cells treated (Figure 5b)

with Ag–PMMA nanocomposite show antagonistic effects as compared to the untreated cells (control) (Figure 5a). Based on FE–SEM analysis, possible mechanisms of bactericidal action may be hypothesized. As shown in micrograph (Figure 5b to 5e) Ag–PMMA nanocomposite treated cells appeared to show atypical shape and a few of the cells were severely damaged (indicated by arrow in Figure 5b). Membrane disruption may increase the cell permeability and permit intracellular material to come out, eventually causing cell death (encircled in Figure 5c and 5e). Sondi reported that, AgNPs have the ability to anchor to the bacterial cell wall and subsequently penetrate it, thereby causing structural changes in the cell membrane like the permeability of the cell membrane and death of the cell.[49] The results clearly designate that the Ag–PMMA nanocomposite is a promising candidate for antibacterial applications due to its dual mode of antibacterial action, contact–killing and release of metal ions.

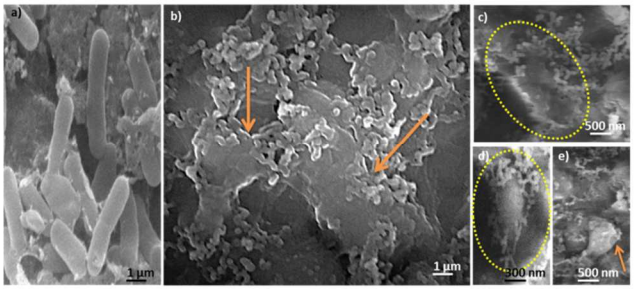

Figure 5 FE–SEM micrographs of *E. coli* bacterial cells (a) untreated (control) and (b–e) treated with Ag–PMMA nanocomposite. Micrographs of (b–e) damaged *E. coli* cells with ruptured morphology.

Ag–PMMA nanocomposite loaded membrane

Treated membrane was prepared by passing the Ag–PMMA nanocomposite solution through membrane using syringe. The membrane changed color from white to yellow after passing Ag–PMMA nanocomposite solution through it (Inset Figure 6b). Characterization of treated membrane was carried out using the DRS, FE–SEM and FTIR. DRS spectrum of treated membrane (Figure S10, Supporting Information) shows peak at 360 nm, which correspond to silver. Optical image of blank membrane (untreated membrane) shows porous nature before treating with nanocomposite, (Figure 6a) while the membrane after treated with Ag–PMMA nanocomposite retains porosity, only color of membrane changed from white to yellow (Figure 6b). The morphology of untreated and treated membrane was determined by FE–SEM (Figure 6c and 6d). FE–SEM micrograph of untreated membrane shows porous morphology (Figure 6c), however the surface of treated membrane was covered with rod shaped nanocomposite. This nanocomposite showed average diameter of 82 nm and 317.4 nm lengths with standard deviation of ±3.7 nm. More FE–SEM images of treated membrane are shown in Figure S11, Supporting Information. FITR study of treated membrane demonstrated that, after loading of Ag–PMMA nanocomposite no shift in the frequencies was observed only the intensity of bands (2978 and 1719 cm^{-1}) changed, which suggests physical adsorption (Figure S12, Supporting Information).

Additionally, the antibacterial activity of treated membrane was investigated against *E. coli* and *S. aureus* using an agar–gel method. The antibacterial properties were measured by evaluating the zone of inhibition around the disk after incubation at 37 °C. Treated membrane (1 cm) shows antibacterial activity with zone of inhibition of 13± 0.33 and 12± 0.57 mm for *E. coli* and *S. aureus* (Figure S13, Supporting Information). This result indicated that treated membrane possesses antibacterial property. However, untreated membrane does not show any antibacterial property (data not shown here).

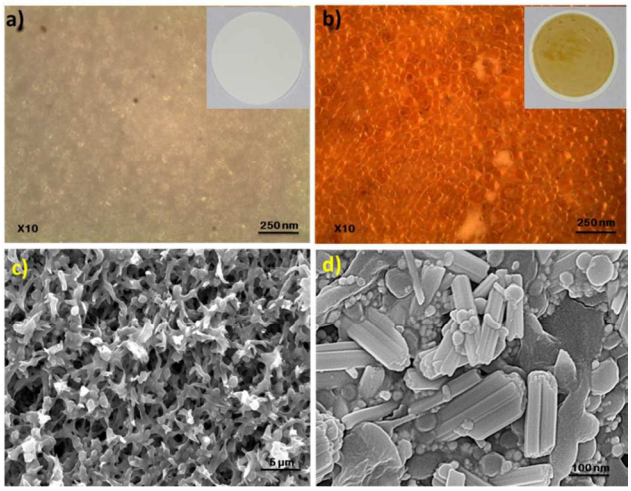

Figure 6 Optical and FE–SEM images of untreated (a, c) and treated membrane (b, d). The inset shows the photographic image of untreated and treated membrane.

Bactericidal effectiveness of treated membrane for water treatment

The treated membrane delivered rapid and effective bactericidal activity as model microorganism present in sludge water was poured through the treated membrane. The average percolation time for 100 mL of sludge water was 10 min. Sludge water contains Gram positive and Gram negative bacteria, was confirmed by microscopy (Figure S14, Supporting Information). When sludge water was passed through untreated membrane (untreated membrane) showed little reduction in bacterial growth (Figure 7b) than original sludge water (Figure 7a). Interestingly, removal of less percentage of microorganisms was achieved by the untreated membrane, which indicates that the membrane without nanocomposite can separate microorganisms to some extent by size exclusion. This result demonstrated that the majority of microorganisms have larger size than the pore size of the membrane. Also, diluted (10 X to 100 X) sludge water was passed through untreated membrane and bacterial growth was evaluated on agar plate (Figure S15, Supporting Information). Sludge water (50 X) was poured through treated and untreated membrane incubated for 24, 48 and 96 h to monitor bacterial growth. However it was observed that untreated membrane shows increase in bacterial growth with time (Figure 7d to 7f). Whereas treated membrane shows reduction in bacterial growth at 24 h and 48 h of incubation (Figure 7g and 7h). Complete deactivation of bacterial growth occurred at 96 h incubation (Figure 7i). Figure 7c depicts absence of Gram positive and Gram negative bacteria in effluent by microbial slide test (72 h–108 h). These results indicated that complete deactivation of bacteria by treated membrane occurred. Consequently, the filter effluent contains dead bacteria, which indicate that treated membrane exhibits antibacterial activity.

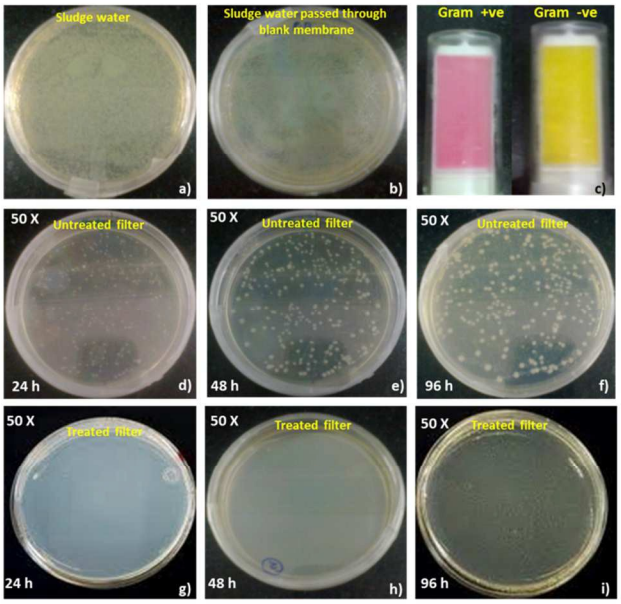

Figure 7 Antibacterial properties of Ag–PMMA nanocomposite loaded membrane. Bacterial growth of (a) sludge water and (b) sludge water passed through blank membrane. (c) Microbial slide test show absence of Gram positive and Gram negative bacteria in effluent water of treated membrane. Bacterial growth of sludge water (50 X) poured through untreated membrane (d to f) and treated membrane (g to i) incubated for 24, 48 and 96 h.

Silver content of the effluent water was analyzed because of possible human health effects from silver exposure in environment and ecosystem.[50] The silver content in the effluent water was 0.09 ppm measured by MP–AES. The quantitative estimation of silver content in effluent of diluted sludge water (10 X to 100 X) of treated membrane was summarized in Table S1, Supporting Information. The acid digestion of the treated membrane (0.1 g) showed silver content 1.19 ppm. While untreated membrane (without passing bacteria through Ag–PMMA loaded membrane) shows silver content 1.28 ppm. However, MP–AES analysis indicated that untreated membrane contains no silver. MP–AES analysis indicates that less amount of leaching of silver (0.1 ppm) from treated membrane, which suggests that Ag–PMMA nanocomposite loaded membrane is suitable for water treatment.

Conclusions

AgNPs were embedded in PMMA matrix by *in–situ* photo assisted polymerization of MMA using AIBN to initiate polymerization process. The fabricated nanocomposite exhibited a lower tendency toward aggregation compared to borohydride synthesized AgNPs. A systematic evaluation of the antibacterial activity of the composite nanoparticles was carried out and showed excellent bactericidal properties against Gram–positive and Gram–negative bacteria. Importantly, deactivation of bacteria by percolation through fabricated nanocomposite loaded membrane occurred. Therefore, the filter effluent contains dead bacteria, which indicates that treated membrane exhibit antibacterial activity. MP–AES analysis estimated that the amount of silver leaching from the treated membrane is less than 0.1 ppm. Although the bactericidal action of Ag–PMMA nanocomposite loaded membrane remains to be tested on large scale. Hopefully, this work will find effective, efficient, and economic method for water treatment.

Acknowledgments

Ms. Shubhangi is thankful to S.P. Pune University for financial support. A. A. Khan/Authors acknowledge the Institute of Bioinformatics and Biotechnology, Savitribai Phule Pune University for providing the infrastructure for conducting biological assays. Authors are also thankful to venture center, NCL, Pune for MP–AES analysis and Ms. Edna Joseph for analysis as well as helpful discussion related to MP–AES. Authors are thankful to UGC–UPE Phase II (Bio–Nano) for financial support. Authors are also thankful to Centre Instrumentation Facility (CIF), SPPU, Pune for FE–SEM analysis.

Notes

† Department of Chemistry, Savitribai Phule Pune University, (Formerly, University of Pune) Ganeshkhind, Pune 411007, India
‡ Department of Chemical Engineering, Indian Institute of Technology Bombay, Powai, Mumbai 400076, India
Corresponding author: Prof. (Mrs.) S. S. Joshi
Department of Chemistry, Savitribai Phule Pune University,Pune – 411007, India
Fax: +91 –020 25691728
Tel: 91020 25601394–573, 569,532
E–mail: ssjoshi@chem.unipune.ac.in

† Electronic Supplementary Information (ESI) available: TEM micrograph, XRD, DLS, TGA, Role of AOT, and Zeta potential of Ag–PMMA nanocomposite, Zone of inhibition, Bacterial growth curve, and MIC plot of Ag– PMMA nanocomposite, DRS spectra and FE–SEM micrographs of treated membrane, FTIR spectra treated and untreated membrane, Zone of inhibition of treated membrane, Microscopy image of Gram positive and Gram negative bacteria, bacterial growth of untreated membrane, and MP–AES analysis of effluent.

Abbreviations

Ag–PMMA, silver–poly (methyl methacrylate)nanocomposite; FTIR, fourier transform infrared spectroscopy; HRTEM, high–resolution transmission electron microscopy; XRD, X–ray diffractometer; FWHM, full width at half maximum; TGA, thermo gravimetric analysis; DLS, dynamic light scattering; DRS, diffuse reflectance spectrophotometry; FE–SEM, field emission scanning electron microscope; MP–AES, microwave plasma–atomic emission spectrometry. MIC, minimum inhibitory concentration; *E. coli*, *Escherichia coli*; *P. aeruginosa*, *Pseudomonas aeruginosa* and *Staphylococcus aureus, S. aureus;* Treated membrane, Ag–PMMA nanocomposite solution was passed through the membrane; Untreated membrane, blank membrane

References

1. Global Risks 2015–Reports–World Economic Forum, reports.*weforum.org/global–risks–2015/press–releases*
2. W. Lee and P. Westerhoff, *Water Research,* 2009, **43**, 2233–2239.
3. H.W. Glaze, *Environ. Sci. Technol.,* 1987, **21**, 224–230.
4. S.P. Mukherjee and K.A. Ray, *Chem. Eng. Technol.,* 1999, **22**, 253−260.

5. K. Gopal, S.S. Tripathy, J.L. Bersillon and S.P. Dubey, *J. Hazard. Mater*., 2007, **140**, 1−6.
6. X. Qu, P.J.J. Alvarez and Q. Li, *Water Res.,* 2013, **47**, 3931−3946.
7. X.L. Qu, J. Brame, Q. Li and J.J.P. Alvarez, *Acc. Chem. Res.*, 2013, **46**, 834−843.
8. F. Meng, S. RChae, A. Drews, M. Kraume and H. S. Shin, *Water Res*., 2009, **43**, 1489−1512.
9. M. Mukherjee and S. De, *Environ. Sci.: Water Res. Technol*., 2015, **1**, 204−217.
10. S. Agnihotri, G. Bajaj and S. Mukherji, *Nanoscale*, 2015, **7**, 7415−7429.
11. N. Musee, M. Thwala and N. Nota, *J. Environ. Monit*., 2011, **13**, 1164−1183.
12. Z. Sheng and Y. Liu, *Water Res.,* 2011, **45**, 6039−6050.
13. A. García, L. Delgado, J.A. Torà, E. Casals, E. González, V. Puntes, X. Font, J. Carrera and A. Sánchez, *J. Hazard. Mater.*, 2012, **199,** 64−72.
14. P. Dallas, V. K. Sharma and R. Zboril, *Adv. Colloid Interface Sci.,* 2011, **166**, 119–135.
15. E. Mahmoudi, L. Y. Ng, M. M. Ba–Abbad and A.W. Mohammad, *Chem. Eng.J*., 2015, **277**, 1−10.
16. M.S. Mauter, Y. Wang, K.C. Okemgbo, C.O. Osuji, E.P. Giannelis and M. Elimelech, *Appl. Mater. Interfaces*., 2011, **3**, 2861−2868.
17. K. Zodrow, L. Brunet, S. Mahendra, D. Li, A. Zhang, Q.L. Li and P.J.J. Alvarez, *Water Res*., 2009, **43**, 715−723.
18. X. Cao, M. Tang, F. Liu, Y. Nie and C. Zhao, *Colloids Surf. B.,* 2010, **81**, 555–562.
19. F. Diagne, R. Malaisamy, V. Boddie, R. Holbrook, B. Eribo and K. Jones, *Environ. Sci. Technol.,* 2012, **46**, 4025–4033.
20. D. Ren and J. Smith, *Environ. Sci. Technol*., 2013, **47**, 3825−3832.
21. J. R. Morones, J. L. Elechiguerra, A. Camacho, K. Holt, J. B. Kouri, J. T. Ramirez and M. J. Yacaman, *Nanotechnology*, 2005, **16**, 2346−2353.
22. S. Taurozzi, H. Arul, V. Z. Bosak, A. F. Burban, T. C. Voice, M. L. Bruening and V. V. Tarabara, *J. Membrane Sci.*, 2008, **325**, 58−68.
23. J. Song, H. Kang, C. Lee, S.H. Hwang and J. Jang, Appl. *Mater. Interfaces*., 2012, **4**, 460−465.
24. J. An, H. Zhang, J. Zhang, Y. Zhao and X. Yuan, *Colloid Polym. Sci*., 2009, **287**, 1425–1434.
25. V. Alt, T. Bechert, P. Steinrücke, M. Wagener, P. Seidel, E. Dingeldein, E. Domann and R. Schnettler, *Biomaterials,* 2004, **18**, 4383−4391.
26. S. Mandal, S. K. Arumugam, R. Pasricha and M. Sastry, *Bull. Mater. Sci.,* 2005, **28**, 503–510.
27. K. M. Abyaneh, S. Jafarkhani and S.K. Kulkarni, *J. Exp. Nanoscience,* 2011, **6**, 159–173.
28. H. J. Kim, H. S. Joo, C. K. Kim, J. Won and S.Y. Kang, *Macromol. Res.,* 2003, **11**, 375–381.
29. P–Y Silvert, R. Herrera–Urbina and K. Tekaia–Elhsissen, *J. Mater. Chem.,* 1997, **7**, 293–299.
30. S. Fukuda, S. Kawamoto and Y. Gotoh, *Thin Solid Films,* 2003, **442**, 117–120.
31. J. Herrero and C. Guillén, *Vacuum*, 2002, **67**, 611–616.
32. Y. Sun, B. Gates, B. Mayers and Y. Xia, *Nano Lett.,* 2002, **2**, 165–168.
33. R. I. MacCuspie, K. Rogers, M. Patra, Z. Suo, J.A. Allen, N.M. Martin and A. VHackley, *J. Environ. Monit*., 2011, **13**, 1212–1226.
34. E.L. Manring, D.Y. Sogah, M. Gordon and M.G. Cohen, *Macromolecule,* 1989, **22**, 4652–4654.
35. S. Hsu, C–W. Chou and S–M. Tseng, *Macromol. Mater. Eng.,* 2004, **289**, 1096–1101.
36. D.N. Singho, A.N. Lah, R.M. Johan and R. Ahmad, *Int. J. Electrochem. Sci.,* 2012, **7**, 5596 –5603.
37. D.N. Singho, M.R. Johan and C.A.N. Lah, *Nanoscale Res. Lett.,* 2014, **9**, 1–6.
38. G. Duan, C. Zhang, A. Li, X. Yang, L. Lu and X. Wang, *Nanoscale Res. Lett.,* 2008, **3**, 118–122.
39. S. Ramesh, H.K. Leen, K. Kumutha and A.K. Arof, *Spectrochim. Acta Part A,* 2007, **66**, 1237–1242.
40. A. Henglein, *Chem. Mater.,* 1998, **10**, 444–450.
41. V. Dal Lago, L. França de Oliveira, K. De Almeida Gonçalves, J. Kobarg and M. Borba Cardoso, *J. Mater. Chem.,* 2011, **21**, 12267−12273.
42. K. Rege, N. R. Raravikar, D.–Y. Kim, L. S. Schadler, P. M. Ajayan and J. Ordick, S. *Nano Lett.,* 2003, **3**, 829–832.
43. R. Kumar and H. Münstedt, *Biomaterials,* 2005, **26**, 2081–2088.
44. W. I. Stephen and A. Townshend, *J. Chem. Soc*., 1965, 3738–3746. Doi: 10.1039/JR9650003118. 573.
45. M.A. Ansari, H.M. Khan, A.A. Khan, A. Malik, A. Sultan, M. Shahid, F. Shujatullah and A. Azam, *Bio. and Med.,* 2011, **3**,141–146.
46. K.A. Ojha, S. Forster, S. Kumar, S. Vats, S. Negi and I. Fischer, *J. Nanobiotechnology*, 2013, **11**, 42–49.
47. Q.L. Feng, J. Wu, G.Q. Chen, F.Z. Cui, T.N. Kim and J.O. Kim, *J. Biomed. Mater.,* 2000, **52**, 662–668.
48. M. Rai, A. Yadav and A. Gade, *Biotechnol. Adv.,* 2009, **27**, 76–83.
49. I. Sondi and B. Salopek–Sondi, *J. Coll. Inter. Sci*., 2004, **275**, 177–182.
50. P. Drake and K. Hazelwood, *Ann. Occup. Hyg*., 2005, **49**, 575–585.

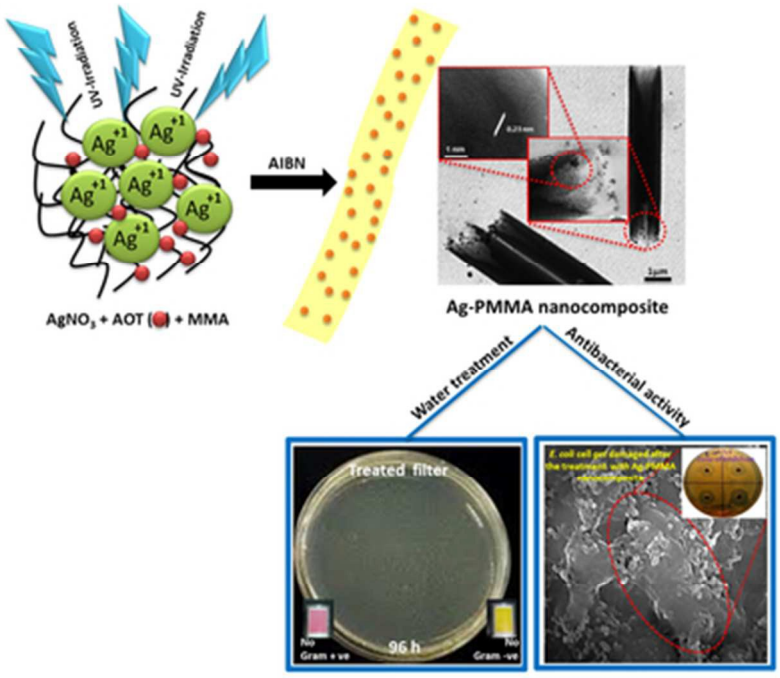

38x31mm (300 x 300 DPI)